PREDICTION OF ICE AND FROST FORMATION IN THE FIN TUBE EVAPORATORS FOR AIR/WATER HEAT PUMPS

M. Albert, R. Sahinagic, L. Gasser, B. Wellig and K. Hilfiker
Lucerne University of Applied Sciences and Arts – Engineering & Architecture,
CC Thermal Energy Systems & Process Engineering,
Technikumstrasse 21, CH-6048 Horw, Switzerland.

In the next few years, the seasonal performance factor of air/water heat pumps will be greatly increased. Success in doing this will depend on two factors: The adaptation of the operating characteristic of the heat pump by the use of continuous power control and the reduction of ice and frost formation. Frost leads to a considerable reduction of the airflow through the evaporator and, therefore, of heat and mass transfer. The formation of ice and frost is influenced by a complex interaction between evaporator, fan characteristic and the characteristic of the heat pump itself. In order to further improve the efficiency of the overall system, a precise prediction of the operation behaviour is required. Based on the theory of simultaneous heat and mass transfer, a mathematical-physical simulation program was developed in the course of the LOREF project. This program allows forecasts of the non-stationary the operation behaviour of the air/water heat pump during ice and frost formation in the evaporator to be made. Here, the greatest challenge was to develop a physical correlation for the properties of the ice and frost deposits during this non-stationary process. Numerous experiments allowed four fields to be distinguished with different characteristics - dependent on the temperature on the boundary layer between air and ice or frost. Comparison with the results of measurements made show that the simulation program developed represents the processes involved in an air/water heat pump during its operation with a high degree of accuracy.

Key Words: ***air/water heat pump, ice and frost formation, simulation***

1 INTRODUCTION

Air/water heat pumps (A/W-HP) extract heat energy from ambient air when this is cooled down in an evaporator in the form of a fin tube heat-exchanger. At low ambient temperatures, the surface temperature of the evaporator falls below the freezing point of water resulting in the water vapour contained in the air being deposited on the fins and tubes in the form of ice or frost. The building up of ice or frost layers leads to an obstruction of the free cross-section in the evaporator and thus reduces the air flow rate; this leads in turn to a degradation of heat transfer and, therefore, of the efficiency of the whole heat pump. The growth of a frost layer leads to non-stationary processes during operation, meaning that process evaluations are heavily impeded; in order to verify the effects of measures taken to optimise the A/W-HP, complex experiments are often unavoidable. In the LOREF project (Berlinger *et al*. 2008), a mathematical-physical simulation program was developed which allowed the calculation of the non-stationary operating behaviour of A/W-HP with ice and frost formation in the evaporator for any geometries. The core of the calculation program is a model for simultaneous heat and mass transfer along with an empirically developed correlation for the calculation of the effective thickness of the frost layer

formed and the air-side heat transfer coefficient. Reliable statements on the behaviour of the entire heat pump process can only be made if it is possible to correctly calculate both the growth of the frost layer and the associated air-side pressure drop across the evaporator.

2 STATE OF THE ART

A layer of frost on the fins of the evaporator has a negative effect on the thermal resistance between ambient air and evaporating working fluid as a result of two different effects. Because of its limited thermal conductivity, the frost represents - together with that of the fin and tube material - an additional thermal resistance between the boundary layer of the air and the evaporating refrigerant. The thermal conductivity of frost is heavily dependant on its density as the air trapped in the pores exhibits a considerably lower thermal conductivity than solid ice. From measurements, it is known that the thermal conductivity of frost can be calculated for the relevant temperature range using $\lambda F = 0.15$ W/mK (Sahinagic *et al.* 2004). The obstruction of the free cross-section has, however, a much greater influence than the higher thermal resistance of the frost layer (Sahinagic *et al.* 2004). As a result of the increased pressure drop, the air flow rate decreases in accordance with operating characteristics of the fan; the output temperature of the air falls and the simultaneous heat and mass transfer is impaired. As a result, the evaporation temperature drops and, along with it, the efficiency of the heat pump. Therefore, the evaporator can be optimised by providing for a more even distribution of the frost deposited. Most studies concerning frost formation in evaporators are concerned with the direct cooling systems in refrigerated warehouses, *i.e.* concerning de-sublimation at low temperatures. Investigations in the temperature range of -10°C to 15°C relevant to A/W-HP are very seldom. For the definition of a model, however, one can revert to the examination of selected works on the subject. Sanders, for example, has applied Merkel's main equation (Merkel 1926) to heat and mass transfer in a fin tube heat-exchanger (Sanders 1974). Using this approach, the temperature and humidity gradients can be united in an enthalpy gradient, which allows a considerable simplification of the equations for simultaneous heat and mass transfer. With the calculation method for heat transfer circuits introduced by Strelow, a non-iterative calculation of the input and output states for the evaporator is possible (Strelow 1997). In this case, the characteristics of the heat exchangers are described on the basis of the operating characteristics according to Bošnjaković (Bošnjaković *et al.* 1997). The calculation of the pressure drop in the dry evaporator according to Glass' simple empirical equation provides very precise results (Glass 1988). Fahlén extended Glass' equation with the effective frost thickness, which means that the pressure drop in an iced-up evaporator can also be evaluated (Fahlén 1996). In this case, the effective frost layer is defined as the thickness of a flat layer which would result in the same pressure drop as the real layer of frost with all its irregularities.

3 MODEL

3.1 Simultaneous heat and mass transfer

The principal equations for simultaneous heat and mass transfer were derived using the example of a duct of infinitesimal length cooled on one side. It must be noted that different states can occur in the evaporator depending on ambient conditions. If the surface temperature of the fins is above the dew point temperature of moist ambient air, the air will be chilled without being dehumidified. At surface temperatures below the dew point temperature, the water vapour in moist air condenses and a latent heat flow occurs in addition to the sensible heat flow obtained from the cooling of the air. Surface temperatures below the freezing point of water lead to direct de-sublimation of water vapour in the air or to the freezing of any condensate present; the latent heat flow is, compared with condensation, increased by the amount of heat released during

solidification.

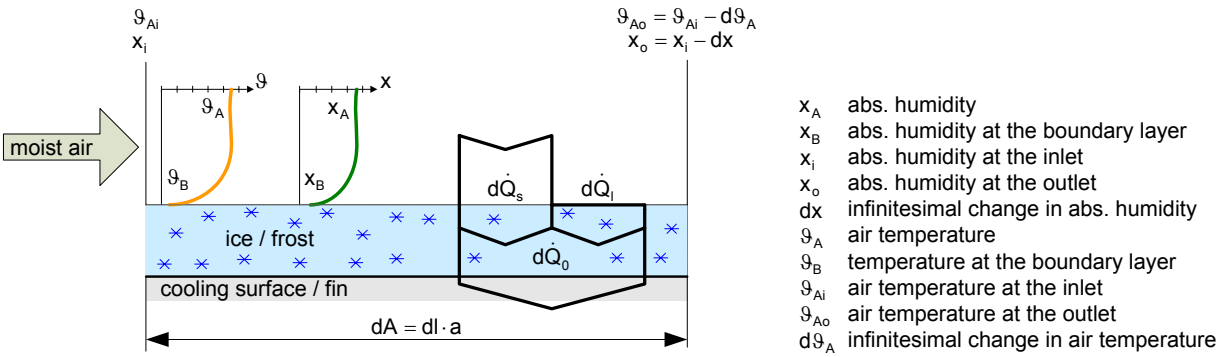

Figure 1: Surface area of infinitesimal length

The entire heat flow transmitted to the cooling surface area $d\dot{Q}_0$ consists of, in total, the sensible heat provided by the cooling of moist air $d\dot{Q}_s$ (convective heat transfer) and the latent heat flow $d\dot{Q}_l$ of the condensation and/or solidification of the water vapour precipitated from the air $d\dot{m}_{spV}$ (mass transfer):

$$d\dot{Q}_s = \alpha_A \cdot (\vartheta_A - \vartheta_B) \cdot dA \tag{1}$$

$$d\dot{Q}_l = r_i \cdot d\dot{m}_{spV} = r_i \cdot \beta \cdot \rho_A \cdot (x_A - x_B) \cdot dA \tag{2}$$

The variable r_i corresponds to the specific enthalpy of evaporation of water r_v during condensate formation and, for frost formation, the specific enthalpy of sublimation r_s.
In accordance with Lewis' analogy, the mass transfer coefficient β and the heat transfer coefficient α_A are proportional to each other. If the Lewis number Le is known, β can be calculated from α_A. For the present application with moist air, one can calculate β using $Le = 1$ (Sahinagic *et al.* 2004).

$$\beta = \alpha_A \cdot \frac{1}{\rho_A \cdot c_{pA}} \cdot \frac{1}{Le^{2/3}} \tag{3}$$

Consequently, it follows for the entire transmitted heat flow that:

$$d\dot{Q}_0 = d\dot{Q}_s + d\dot{Q}_l = \left[\alpha_A \cdot (\vartheta_A - \vartheta_B) + \frac{\alpha_A}{c_{pA}} \cdot (x_A - x_B) \cdot r_i \right] \cdot dA \tag{4}$$

For the calculation of the simultaneous heat and mass transfer, both the temperature and humidity gradients must be considered. Merkel showed that the two gradients can be formulated in a combined way as an enthalpy gradient (Merkel 1926). The equations for the calculation of simultaneous heat and mass transfer are simplified considerably by the use of enthalpy gradients and a clear overview results. Moreover, the entry state of the air can also be expressed in just one expression, *i.e.* the specific enthalpy of moist air. Merkel starts with equation (4) as the basis of his derivation. In this case, assumptions were made that the Lewis number is one ($Le = 1$) and the specific heat capacities of moist and dry air are approximately identical.

Assuming $c_{pA} \approx c_{pAd}$ the specific enthalpy of moist air is:

$$h_A = c_{pA} \cdot \vartheta_A + x_A \cdot r_v \tag{5}$$

Accordingly, the specific enthalpy gradient between the air and the boundary layer (with saturated air at the boundary layer) is:

$$h_A - h_{sB} = c_{pA} \cdot (\vartheta_A - \vartheta_B) + r_v \cdot (x_A - x_B) \tag{6}$$

Using (6) in (4), the heat flow $d\dot{Q}_0$ results in the case of partial condensation:

$$d\dot{Q}_0 = \frac{\alpha_A}{c_{pA}} \cdot (h_A - h_{sB}) \cdot dA \tag{7}$$

In above equation, the heat flow from the solidification of the water vapour must additionally be added during ice and frost formation.
So that the entire calculation can be made using only enthalpies, all temperatures (internal/external tube surface temperature, evaporation temperature of the working fluid) must also be expressed in terms of their corresponding specific enthalpies. This is done by the use of the specific saturation enthalpy of moist air as the enthalpy in the case of saturation is only dependent on the temperature.
The sensitive heat flow $d\dot{Q}_s$ can be calculated in accordance with (1), or by means of the energy balance over the surface area dA (temperature change $d\vartheta_A$ of moist air while flowing over dA). Thus the following is obtained for α_A :

$$\alpha_A = \frac{\dot{m}_A \cdot c_{pA}}{\vartheta_A - \vartheta_B} \cdot \frac{d\vartheta_A}{dA} \tag{8}$$

For the entire heat flow, with (8) in (7), the following results:

$$d\dot{Q}_0 = \dot{m}_A \cdot \frac{(h_A - h_{sB})}{\vartheta_A - \vartheta_B} \cdot d\vartheta_A \tag{9}$$

The heat flow $d\dot{Q}_0$ is therefore proportional to the quotient of the driving enthalpy and temperature gradients to the boundary layer as well as to the temperature decrease of moist air in the direction of flow. The heat flow $d\dot{Q}_0$ can also be calculated using the air-side energy balance with the infinitesimal change in specific enthalpy of the moist air dh_A :

$$d\dot{Q}_0 = \dot{m}_A \cdot dh_A \tag{10}$$

Using (10) in (9) it follows that:

$$\frac{dh_A}{h_A - h_{sB}} = \frac{d\vartheta_A}{\vartheta_A - \vartheta_B} \tag{11}$$

Assuming that the moist air in the air cooler of the heat pump is saturated, the following is valid:

$$\frac{dh_{sA}}{h_{sA} - h_{sB}} = \frac{d\vartheta_{sA}}{\vartheta_{sA} - \vartheta_B} \tag{12}$$

If the air is saturated with water vapour, its specific enthalpy only depends on its temperature. For simplification, the saturation curve for moist air (Mollier - diagram) is linearised for the relevant temperature range:

$$h_{sA} = a + b \cdot \vartheta_{sA} \tag{13}$$

The relationship between the gradient of the specific saturation enthalpy and the temperature gradient in the direction of flow is then:

$$\frac{dh_{sA}}{d\vartheta_{sA}} = b \tag{14}$$

By differentiation of the specific enthalpy of moist air against saturation temperature, the following results:

$$\frac{dh_{sA}}{d\vartheta_{sA}} = c_{pA} + c_{pV} \cdot x_{sA} + (r_v + c_{pV} \cdot \vartheta_{sA}) \cdot \frac{dx_{sA}}{d\vartheta_{sA}} \tag{15}$$

Since $x_{sA} = x_{sA}(p_{sV}(\vartheta_{sA}))$ it follows that:

$$\frac{dx_{sA}}{d\vartheta_{sA}} = \frac{dx_{sA}}{dp_{sV}} \cdot \frac{dp_{sV}}{d\vartheta_{sA}} \tag{16}$$

From the calculation of the mass loading of the air with water vapour one obtains

$$\frac{dx_{sA}}{dp_{sV}} = \frac{R_A}{R_V} \cdot \frac{1}{p} \tag{17}$$

where R_A is the gas constant for air and R_V the gas constant of water vapour, respectively. From the Clausius-Clapeyron equation for the vapour pressure curve we obtain:

$$\frac{dp_{sV}}{d\vartheta_{sA}} = \frac{r_v \cdot p_{sV}}{R_V \cdot T_{sA}^{\ 2}} \tag{18}$$

By the introduction of (16), (17) and (18) in (15) one obtains:

$$\frac{dh_{sA}}{d\vartheta_{sA}} = c_{pA} + c_{pV} \cdot x_{sA} \cdot (r_v + c_{pV} \cdot \vartheta_{sA}) \cdot \frac{R_A}{R_V^{\ 2}} \cdot \frac{p_{sV}}{p} \cdot \frac{r_v}{T_{sA}^{\ 2}} \tag{19}$$

$c_{pV} \cdot x_{sA}$ and $c_{pV} \cdot \vartheta_{sA}$ can be neglected in comparison to the specific enthalpy of evaporation r_v. For the gradient b the following clear relationship can be formulated:

$$b = \frac{dh_{sA}}{d\vartheta_{sA}} = c_{pA} + \frac{R_A}{R_V^2} \cdot \frac{p_{sV}}{p} \cdot \frac{r_v^2}{T_{sA}^2} \tag{20}$$

3.2 Calculation method for fin tube air coolers (operating characteristic)

For the calculation of the heat exchanger configuration, a method based on coupled matrix equations is applied which allows an iteration-free calculation method to be used that can be applied to any configuration variants. This method was already proposed by Bošnjaković and later further developed by Strelow (Bošnjaković *et al.* 1997, Strelow 1997). With the operating characteristics of the moist air and the working fluid (refrigerant) derived below, it is possible to describe the connection between specific entry and exit enthalpies of both flows in the heat exchanger using a linear approach.
With the aid of the factor b (equation 14), the temperature gradient between the internal surface area of the tube and the evaporating working fluid ($\vartheta_T - \vartheta_R$) can be expressed using the gradient of specific enthalpies $h_{sT} - h_{sR}$ (specific saturation enthalpies). Using the heat transfer coefficient α_R on the working fluid side, the following is valid:

$$d\dot{Q}_0 = \alpha_R \cdot (\vartheta_T - \vartheta_R) \cdot dA = \frac{\alpha_R}{b} \cdot (h_{sT} - h_{sR}) \cdot dA \tag{21}$$

The heat transfer between the moist air and the evaporating working fluid can be calculated with the gradient of specific enthalpies:

$$d\dot{Q}_0 = k(h_A - h_{sR}) \cdot dA \tag{22}$$

For the overall heat transfer coefficient k the following is valid:

$$k = \left(\frac{c_{pA}}{\alpha_A} + \frac{\delta_T}{\lambda_T} + \frac{b}{\alpha_R} \right)^{-1} \tag{23}$$

The entire heat flow $d\dot{Q}_0$ can also be calculated using the energy balances of the two mass flows over the surface area dA. In this case, the changes in the vapour quality x_V and temperature ΔT_R on the working fluid side must be considered due to the temperature glide and the flow-dependent pressure drop. The energy balances of the two fluid flows give for the transferred heat flow:

$$d\dot{Q} = \dot{m}_{Ad} \cdot dh_A = \dot{m}_R \cdot r_{vR} \cdot dx_V = \frac{\dot{m}_R \cdot \tilde{c}_{pR}}{b} \cdot dh_{sR} \tag{24}$$

With the corrected specific heat capacity:

$$\tilde{c}_{pR} = \frac{r_{vR} \cdot (1 - x_V)}{\Delta T_R} \tag{25}$$

The factor $X = A / A_0$ indicates the relationship between a part-surface area A to the total air-side heat transfer surface area A_0. Using this together with $Y = (h_A - h_{sR})$, it follows that:

$$\dot{U}_A \cdot dh_A = k \cdot A_0 \cdot Y \cdot dX \text{ and } \dot{U}_R \cdot dh_{sR} = k \cdot A_0 \cdot Y \cdot dX \tag{26}$$

With corrected mass flows $\dot{U}_A$ and $\dot{U}_R$:

$$\dot{U}_A = \dot{m}_{Ad} \text{ and } \dot{U}_R = \frac{\dot{m}_R \cdot \tilde{c}_{pR}}{b} \tag{27}$$

By rearranging the equations in (26) one obtains:

$$\frac{dh_A}{dX} = \frac{k \cdot A_0}{\dot{U}_A} \cdot Y \text{ and } \frac{dh_{sR}}{dX} = \frac{k \cdot A_0}{\dot{U}_R} \cdot Y \tag{28}$$

The above equations are subtracted from each other:

$$\frac{dY}{dX} + \left(\frac{k \cdot A_0}{\dot{U}_R} - \frac{k \cdot A_0}{\dot{U}_A} \right) \cdot Y = 0 \tag{29}$$

For a counter-flow heat exchanger with $X = 0$ one obtains the exit state ($h_A = h_{Ao}$) for the specific enthalpy of moist air along with the entry state ($h_{sR} = h_{sRi}$) for the working fluid on entry into the evaporator. The integration of (29) then yields:

$$Y = (h_A - h_{sR}) = (h_{Ao} - h_{sRi}) \cdot e^{\left[-\left(\frac{k \cdot A_0}{\dot{U}_R} - \frac{k \cdot A_0}{\dot{U}_A} \right) \cdot X \right]} \tag{30}$$

For $X = 1$ the following is valid:

$$h_{Ai} - h_{sRo} = (h_{Ao} - h_{sRi}) \cdot e^{\left[-\left(\frac{k \cdot A_0}{\dot{U}_R} - \frac{k \cdot A_0}{\dot{U}_A} \right) \right]} \tag{31}$$

The total transferred heat flow is:

$$\dot{Q}_0 = \dot{U}_A \cdot (h_{Ai} - h_{Ao}) = \dot{U}_R \cdot (h_{sRo} - h_{sRi}) \tag{32}$$

From (31) and (32), one obtains the dimensionless change in specific enthalpy of the two streams:

$$\phi_{hA} = \frac{(h_{Ai} - h_{Ao})}{(h_{Ai} - h_{sRi})} = \frac{1 - e^{\left[-\left(\frac{k \cdot A_0}{\dot{U}_{AF}} - \frac{k \cdot A_0}{\dot{U}_L} \right) \right]}}{1 - \frac{\dot{U}_L}{\dot{U}_{AF}} \cdot e^{\left[-\left(\frac{k \cdot A_0}{\dot{U}_R} - \frac{k \cdot A_0}{\dot{U}_A} \right) \right]}} \text{ and } \phi_{hR} = \frac{\dot{U}_A \cdot \phi_{hA}}{\dot{U}_R} \tag{33}$$

Using the same method, the operational characteristics for a finned tube element with a finite surface area were subsequently derived. In this case, a fin efficiency must be taken into account

during the consideration of heat transfer from moist air to the fins of a tube element, which is calculated according to Sanders (Sanders 1974). The calculation of the air-side heat transfer coefficient is carried out using an empirical correlation obtained from measurements on the dry evaporator (VDI-Wärmeatlas 2006). By stringing several tube elements together, one finally obtains a complete fin tube evaporator. The combination of the tube elements that are considered as being single units is done in the calculation program using a so-called structure matrix.

3.3 Empirical correlations

As already mentioned, the main effect of a frost layer is the obstruction of the free cross-section for air-flow in the evaporator, which leads to a reduction of the air flow rate account of the fan characteristic. For this reason, the precise calculation of the pressure drop is especially important for the correct simulation of the whole process. the pressure drop for a dry fin tube evaporator (Fahlén 1996) is:

$$\Delta p_0 = 5 \cdot \frac{n_T}{s_{Fin}} \cdot \rho_A \cdot {w_A}^2 \tag{34}$$

This equation contains only the number of the tube rows n_T in the direction of air flow, the fin spacing s_{Fin}, the density of moist air ρ_A and the air velocity between the fins w_A. An evaluation of the equation for air velocities between 1 and 3 m/s yielded a maximum deviation of 10% (Berlinger *et al.* 2008). Using the continuity equation, the pressure drop can be expressed as a function of the air flow rate $\dot{V}_{A0}$ (valid for a dry evaporator). In this case, the number of the fins n_{Fin} and the height of the evaporator H are required as additional factors.

$$\Delta p_0 = 5 \cdot \frac{n_T}{{n_{Fin}}^2 \cdot H^2} \cdot \rho_A \cdot \frac{{\dot{V}_{A0}}^2}{{s_{Fin}}^3} \cdot 10^{-3} \tag{35}$$

Reduction of the flow cross-section by the effective thickness of the frost layer δ_F:

$$\Delta p_F = 5 \cdot \frac{n_T}{{n_{Fin}}^2 \cdot H^2} \cdot \rho_{fL} \cdot \frac{{\dot{V}_A}^2}{(s_{Fin} - 2 \cdot \delta_F)^3} \cdot 10^{-3} \tag{36}$$

Solving equation (35) for s_{Fin}, inserted in (36) and solved for the effective frost thickness:

$$\delta_F = \left(\frac{0.625 \cdot 10^{-3} \cdot n_T \cdot \rho_A}{{n_{Fin}}^2 \cdot H^2} \right)^{\frac{1}{3}} \cdot \left(\frac{{\dot{V}_{A0}}^{\frac{2}{3}}}{{\Delta p_0}^{\frac{1}{3}}} - \frac{{\dot{V}_A}^{\frac{2}{3}}}{{\Delta p_F}^{\frac{1}{3}}} \right) \tag{37}$$

In order to be able to determine the effective frost thickness from the frost mass deposited, an empirical correlation was developed on the basis of an extensive set of measurements of the effective frost thickness as a function of the frost mass loading. In this case, the effective frost thickness is calculated from measured values for the pressure drop Δp_F and the air flow rate $\dot{V}_A$ using equation (37). By simultaneous measurement of humidity at the input and output of the evaporator, the frost mass m_F, and, by dividing by the evaporator surface area A_0, the frost mass loading m_{aF} can be calculated. The results of the measurements are shown in figure 2 for various fin temperatures.

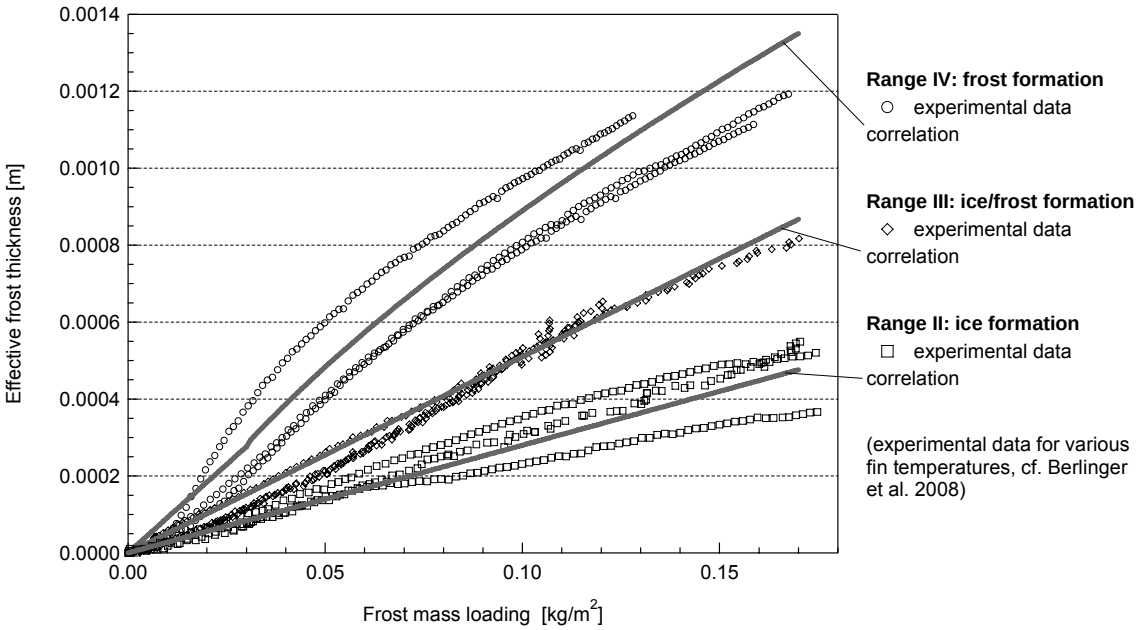

Figure 2: Effective frost thickness as a function of the frost mass loading in different ranges

Since the frosting process depends strongly on the fin temperature, four different ranges can be distinguished for which a separate correlation is necessary. The different correlations are summarised in table 1.

Table 1: Correlations for the effective frost thickness for various temperature ranges

Range	ϑ_{Fin}	Correlation	Illustration
I Condensate formation	> -3°C	$\frac{\Delta p_C}{[Pa]} = \frac{\Delta p_0}{[Pa]} \cdot \left(1 + 7.2 \cdot \frac{m_{aC}}{[kgm^{-2}]}\right)$	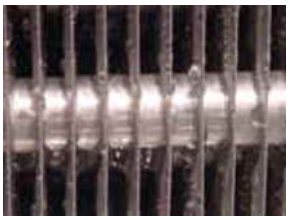
II Ice formation	-4.1…-3°C	$\frac{\delta_F}{[m]} = 0.0028 \cdot \frac{m_{aF}}{[kgm^{-2}]}$	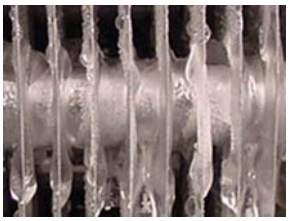
III Ice/frost formation	-5.5…-4.1°C	$\frac{\delta_F}{[m]} = 0.0051 \cdot \frac{m_{aF}}{[kgm^{-2}]}$	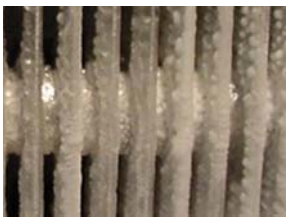

IV Frost formation	< -5.5°C	For $m_{aF} \leq 0.03\ kgm^{-2}$ $\frac{\delta_F}{[m]} = 0.0092 \cdot \frac{m_{aF}}{[kgm^{-2}]}$ For $m_{aF} > 0.03\ kgm^{-2}$ $\frac{\delta_F}{[m]} = 0.0051 \cdot \frac{m_{aF}^{0.65}}{[kgm^{-2}]} - 0.0002$	

In area I, the water vapour is just condensed without any freezing occurring. The condensate forms a film or individual drops on the fins through which the air-side flow pressure drop is increased. As the condensate flows off continuously, a steady state is achieved after a certain period of time. At the somewhat lower fin temperatures occurring in area II, the condensate no longer flows off but, with a slight delay, freezes to a compact ice layer. The transitional area between ice and frost formation is covered in area III. As a result of small local temperature differences, both ice and frost can result. Area IV applies to very low fin temperatures where a frost layer is formed from the beginning as a result of pure de-sublimation. As the increase in the effective frost thickness is not linear (figure 2), two different correlations are used depending on the frost mass loading.
For the calculation of the overall heat transfer coefficient in (23), the air-side heat transfer coefficient α_A is required. The empirical correlation created for this is based on a calculation method for ribbed surfaces (VDI-Wärmeatlas 2006). The equation for calculation of the apparent heat transfer coefficient α_{app} is:

$$\frac{1}{k} = \frac{1}{\alpha_{app}} + \frac{A_0}{A_{Ti}} \cdot \left(\frac{1}{\alpha_{CB}} + \frac{\delta_T}{\lambda_T} \right) \tag{38}$$

The overall heat transfer coefficient k was determined by measurement on a brine cooled fin tube heat-exchanger under dry conditions. The heat conduction through the tube wall is calculated from the wall-thickness δ_T and the thermal conductivity λ_T of the tube material. The heat transfer coefficient of the cold brine α_{CB} can be taken from literature (VDI-Wärmeatlas 2006). The heat transfer relation of the cold brine and the heat conduction through the tube wall are weighted by the surface area ratio between the air-side surface A_0 and the internal surface area of the tube wall A_{Ti}. For the calculation of the actual heat transfer coefficient, the fin efficiency must be considered. The following relationship between α_A and α_{app} is valid:

$$\alpha_{app} = \alpha_A \cdot \left[\frac{A_{Te}}{A_0} + \eta_{Fin} \cdot \frac{A_{Fin}}{A_0} \right] \tag{39}$$

For the air side heat transfer coefficient the following empirical correlation is valid (Berlinger *et al.* 2008):

$$\alpha_A = 45 \cdot w_A^{0.78} \tag{40}$$

4 RESULTS

The pressure drop represents the main factor in simulations since the course of the process over time is significantly determined by it. Especially in the case of a flat fan characteristic, a small deviation in the calculation of pressure drop has a strong effect on the air flow rate and therefore on the heat transfer in the evaporator too. Moreover, the air flow rate influences frost growth, thus leading to an over-proportionate error in the simulated pressure drop. As an example, figure 3 shows a comparison between measurements and simulation for air temperatures of 6°C and -2°C and a relative humidity of 80%. A detailed description of the heat exchanger and the experiments can be found in Berlinger *et al.* (2008).

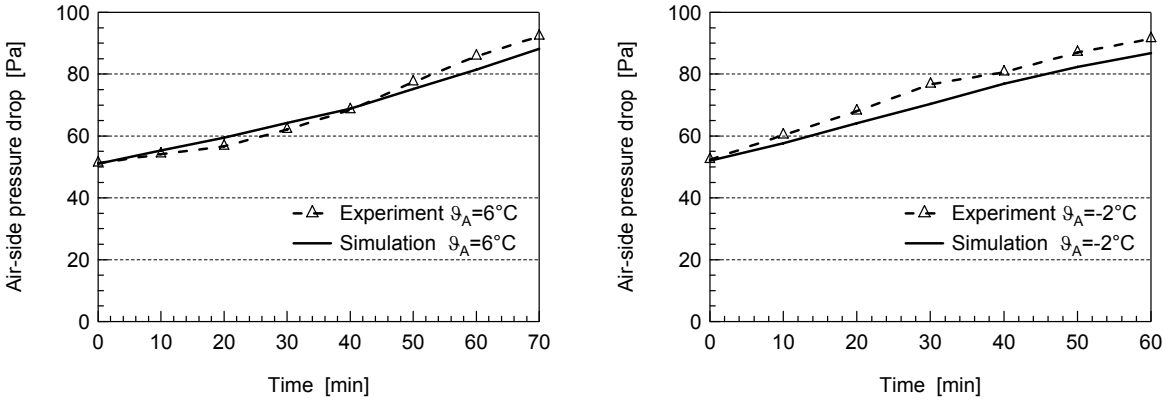

Figure 3: Air-side pressure drop over time at 6°C and -2°C with 80% rH

In all operating states, the air-side pressure drop can be simulated with a high degree of accuracy. The maximum discrepancy in comparison to measured values is around 8%. The simulated pressure drops are tendentially somewhat too low. The measured and simulated values for heat flows in the evaporator over time are shown in figure 4 at air temperatures of 6°C and -2°C and a relative humidity of 80%.

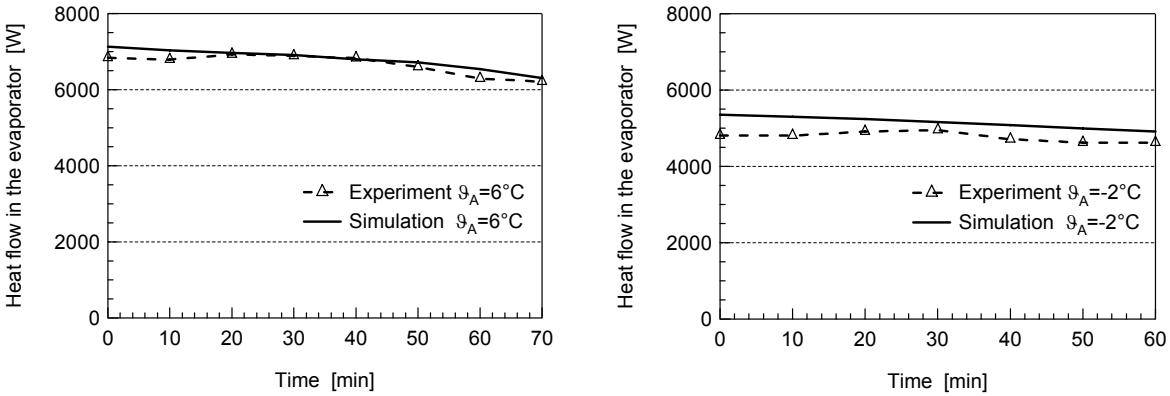

Figure 4: Heat flow in the evaporator over time at 6°C and -2°C with 80% rH

The validation of the simulation program was carried out using the results of measurements made in experiments with a commercial A/W-HP (Sahinagic *et al.* 2008).

5 CONCLUSIONS AND OUTLOOK

Using the simulation program described, the non-stationary operating behaviour of an A/W-HP can be represented with a high accuracy. As a result, the effects of optimisation measures taken on the heat pump can be estimated with little effort and, consequently, the number of measurement series required can be greatly reduced. Especially during the development of control concepts for continuously power-controlled A/W-HP, a simulation program can be of great benefit since the icing-up of the heat pump also varies on account of changing operating characteristics. Here, new control concepts can be tested in a virtual way and any possible weaknesses can be recognised at an early stage. Moreover, plant-specific control system parameters can be determined in advance.

6 REFERENCES

Berlinger L., M. Imholz, M. Albert, B. Wellig, K. Hilfiker 2008. LOREF: Optimierung des Lamellenluftkühlers/Verdampfers von Luft/Wasser-Wärmepumpen, Teil 1: Theoretische und experimentelle Untersuchungen, Swiss Federal Office of Energy, Berne.

Bošnjaković F, K.F. Knoche 1997. Technische Thermodynamik, 2. Teil, 6. Auflage, Dr. Dietrich Steinkopff Verlag, Darmstadt.

Fahlén P. 1996. Frosting and Defrosting of Air Coils, Doctoral Thesis, Document D36, Department of Building Services Engineering, Chalmers University of Technology, Göteborg.

Glas L.O. 1988/1989. Operation experience from air-water heat pumps – Operational comparisons.

Merkel F. 1926. “Verdunstungskühlung”, VDI-Zeitschrift 70, S. 123-128.

Sahinagic R., M. Imholz, L. Berlinger, H. Huber, K. Hilfiker 2004. LOREF: Untersuchung der Frostbildung für Lamellenluftkühler von Wärmepumpen, Swiss Federal Office of Energy, Berne.

Sahinagic R., L. Gasser, B. Wellig, K. Hilfiker 2008. LOREF: Optimierung des Lamellenluftkühlers/Verdampfers von Luft/Wasser-Wärmepumpen, Teil 2: Mathematisch-physikalische Simulation des Lamellenluftkühlers mit Kondensat- und Frostbildung, Swiss Federal Office of Energy, Berne.

Sanders C.Th. 1974. Frost Formation: The influence of frost formation and defrosting on the performance on air coolers, Dissertation WTHD 63, Delft University of Technology, Delft.

Strelow O. 1997. “Eine allgemeine Berechnungsmethode für Wärmeübertragerschaltungen”, Forschung im Ingenieurwesen, Vol. 63, Part 9, S. 255-261.

VDI-Wärmeatlas 2006. Verein Deutscher Ingenieure, 10. bearbeitete und erweiterte Auflage, Springer-Verlag, Berlin, Heidelberg, New York.